Effect of magnetism and atomic order on static atomic displacements in the Invar alloy Fe-27 at.% Pt

C. R. Sax,[1] B. Schönfeld,[1] and A. V. Ruban[2,3]

[1]*Laboratory of Metal Physics and Technology, Department of Materials, ETH Zurich, 8093 Zurich, Switzerland*

[2]*Department of Materials Science and Engineering, Royal Institute of Technology, 10044 Stockholm, Sweden*

[3]*Materials Center Leoben Forschung GmbH, A-8700 Leoben, Austria*

(Received 23 April 2015; published 24 August 2015)

Fe-27 at.% Pt was aged at 1123 K and quenched to room temperature (RT) to set up a state of thermal equilibrium. The local atomic arrangement was studied by diffuse x-ray scattering above (at 427 K) and below (at RT) the Curie temperature as well as at RT under a saturating magnetic field. The separated short-range order scattering remained unchanged for all three states, with maxima at 100 positions. Effective pair interaction parameters determined by the inverse Monte Carlo method gave an order-disorder transition temperature of about 1088 K, close to direct experimental findings. The species-dependent static atomic displacements for the first two shells show large differences, with a strong increase in magnitude from the state at 427 K over RT to the state under saturating magnetic field. This outcome is in agreement with an increase in atomic volume of Fe with increasing local magnetic moment. Electronic-structure calculations closely reproduce the values for the static atomic displacements in the ferromagnetic state, and predict their dependence on the atomic configuration. They also reveal a strong dependence of the magnetic exchange interactions in Fe-Pt on the atomic configuration state and lattice parameter. In particular, the increase of the Curie temperature in a random state relative to that in the ordered one is demonstrated to be related to the corresponding change of the magnetic exchange interactions due to the different local atomic chemical environment. There exists a similar strong concentration dependence of the chemical interactions as in the case of magnetic exchange interactions. Theoretical effective interactions for Fe-27 at.% Pt alloy are in good agreement with experimental results, and they also reproduce well the $L1_2$-A1 transition temperature.

DOI: 10.1103/PhysRevB.92.054205 PACS number(s): 64.60.Cn, 71.15.−m, 75.50.Bb

I. INTRODUCTION

The Invar effect is characterized through a very low thermal expansion over an extended temperature range. It was discovered by Guillaume in 1897 (Ref. [1]) on Fe-35 at.% Ni that showed a thermal expansion coefficient being by one order of magnitude lower than the values of the pure elements. The same anomaly was found later on in numerous materials with different crystallographic structures, degrees of order, or binding states. The only similarity among all Invar materials was that they were magnetically active and that the effect occurred around and up to the Curie temperature [2].

First-principles calculations of ferromagnetic Invar systems have explained why this effect happens in the ferromagnetic state close to the Curie temperature when the magnetization is substantially reduced: the reduction of the magnetization with increasing temperature is accompanied by a noticeable decrease of the magnitude of the local magnetic moment thereby reducing magnetic pressure, the drop of which compensates for the thermal lattice expansion due to anharmonic effects in the lattice vibrations [3–6].

An *ab initio* study of species-dependent static atomic displacements of Fe-35 at.% Ni in Ref. [7] has demonstrated that this picture is very well reproduced locally. First of all, larger displacements between Fe-Fe nearest neighbors are obtained in the ferromagnetic state than in the "ferrimagnetic" state, which has been used to model a ferromagnetic state with a reduced magnetization. The magnetic moment on Fe atoms in such a ferrimagnetic state is substantially reduced compared to those in the ferromagnetic state. Second, the distance between Fe atoms in both states tends to expand with increasing moment for fixed local coordinations in both magnetic states.

Diffuse x-ray scattering studies were done by Robertson *et al.* [8] to determine the static atomic displacements in Fe-36.8 at.% Ni. The alloy, in a short-range ordered state, was investigated at two temperatures (293 and 60 K), both being below the Curie temperature. The 3λ method [9] was applied which is well suited to analyze the microstructure of alloys with neighboring elements in the periodic table. It also allows the contributions that do not depend on the scattering contrast (thermal diffuse scattering, Huang scattering, and Compton scattering) to be separated experimentally from those that depend on it (short-range order scattering and displacement scattering). Static atomic displacements up to the 8th shell were determined within the radial approximation. They were stronger in magnitude at 60 K than at 293 K while the sign remained unchanged. Line scans of the diffuse intensity of the non-Invar alloy Fe-53.5 at.% Ni at 30 and 293 K on the other hand did not give any indication for temperature-sensitive displacements [10].

Based on short-range order parameters of Fe-36.8 at.% Ni in a state as quenched from 753 K, Robertson *et al.* [8] stated that Fe tends to form platelets on {100} planes. These platelets have to be very small and/or rare due to the small value of the nearest-neighbor short-range order parameter (only about a tenth of the maximum achievable magnitude). Based on elastic diffuse neutron scattering around Bragg reflections of Fe-(35 to 60) at.% Ni in the as-grown state, Tsunoda *et al.* [11] also noted a heterogeneity in the Fe-Ni system. Two explanations of these heterogeneities were provided: (i) formation of Fe-rich clusters in the high-volume state and (ii) formation of embryos of the fcc to bcc martensitic transformation at low temperatures [2].

With respect to structural aspects such as low-temperature order or ground states, Fe-Ni, Fe-Pt, Fe-Pd are often compared to one another (see, e.g., Barabash *et al.* [12]). All three systems have in common that they are Invar alloys [2,13]. The Invar system Fe-Pt differs in various aspects from Fe-Ni that was studied in much detail, e.g., it shows no deviation from the Slater-Pauling curve and there is no mixed magnetic behavior. Concerning the Fe-Pd system, one should note that a two-phase state is present in thermal equilibrium and that single crystals of larger "mosaicity" are typically grown.

The magnetovolume effects of Fe-Pt were studied by Sumiyama *et al.* [14] for ordered and disordered Fe-(28 to 32) at.% Pt. A negative linear thermal expansion coefficient was found for both states around the Curie temperature, larger in the disordered state and for lower Pt fractions (e.g., $T_c^{\mathrm{ord}} = 505$ K, $T_c^{\mathrm{disord}} = 371$ K for Fe-28 at.% Pt, see also Ref. [15]). Spontaneous volume magnetostriction at 0 K as well as forced magnetostriction were larger for the disordered than the ordered state and increased with lower Pt fraction. The same dependence for the spontaneous volume magnetostriction was found by *ab initio* calculations using the disordered local moment approach [5].

Evidence for further magnetic transitions in Fe-Pt was obtained by Matsushita *et al.* [16,17] performing pressure studies on disordered Fe-30 at.% Pt and ordered Fe-27.2 at.% Pt up to 7.5 GPa. With increasing pressure, the Curie temperature was observed at considerable lower temperature than at ambient pressure and transitions to high-pressure magnetic states for both the ordered and the disordered phases were found at low temperatures based on ac susceptibility measurements.

Diffuse neutron scattering in ordered Fe-28 at.% Pt was investigated by Tsunoda *et al.* [18]. A butterfly-shaped pattern around the 200 fundamental peak position (dominantly of nuclear character, reflecting lattice deformations) was found below the Curie temperature. As in the case of Fe-36.8 at.% Ni this diffuse scattering pattern was attributed to premartensitic embryos evolving due to the martensite transformation below room temperature (RT) [19,20]. The pattern around the 100 superstructure reflection (dominantly of magnetic character, thus reflecting the spin arrangement) was of circular shape. Note that there are different types of a martensite phase depending on the degree of long-range order of the high-temperature parent phase: with increasing order it changes from bcc to bct to fct (with lattice parameter ratio $c/a < 1$) to fct (with $c/a > 1$) [21].

The aim of this paper is to study the Invar anomaly on the atomic level from diffuse x-ray scattering and by *ab initio* calculations. As there is only one genuinely magnetic constituent, Fe-Pt is simpler than Fe-Ni addressed before. The strong and even negative thermal expansion below the Curie temperature will provide much larger displacements than in the case of Fe-Ni. By doing experiments around the Curie temperature and exploiting the strong forced volume magnetostriction, states in a close temperature range may be evaluated introducing less experimental uncertainty in considering thermal diffuse scattering. The strong dependence of the local magnetic moment on the magnetic and chemical states will be addressed by calculating the magnetic transition temperatures in dependence of the chemical state as well as the order-disorder transition and comparing those temperatures with direct experimental data.

For this study, short-range ordered Fe-27 at.% Pt was chosen for three reasons: (i) with 27 at.% Pt it is assured that no martensite will be present at room temperature and above, (ii) for this composition and for the short-range ordered state the anomaly in thermal expansion is largest and (iii) excellent crystal quality will also allow the near-surface microstructure to be investigated as a further way to possibly vary the microstructure (not the topic of the present investigation).

II. METHODOLOGY

A. Basics of elastic diffuse scattering

Elastic diffuse scattering from a binary (here Fe-Pt) alloy is separated into the contributions of short-range order scattering $I_{\mathrm{SRO}}(\mathbf{h})$, size-effect scattering $I_{\mathrm{SE}}(\mathbf{h})$, and Huang scattering $I_{\mathrm{H}}(\mathbf{h})$ at any position with scattering vector $\mathbf{h}$. The first two contributions are (for details, see Refs. [22–26])

$$\begin{aligned} I_{\mathrm{SRO}}(\mathbf{h}) &= \sum_{lmn} \alpha_{lmn} \cos(\pi h_x l) \cos(\pi h_y m) \cos(\pi h_z n), \\ I_{\mathrm{SE}}(\mathbf{h}) &= \mathbf{h} \cdot [\eta \mathbf{Q}^{\mathrm{PtPt}}(\mathbf{h}) + \xi \mathbf{Q}^{\mathrm{FeFe}}(\mathbf{h})], \end{aligned} \tag{1}$$

where, e.g.,

$$\begin{aligned} Q_x^{\mathrm{PtPt}}(\mathbf{h}) &= -2\pi \sum_{lmn} (c_{\mathrm{Pt}}/c_{\mathrm{Fe}} + \alpha_{lmn}) \langle x_{lmn}^{\mathrm{PtPt}} \rangle \\ &\quad \times \sin \pi h_1 l \ \cos \pi h_2 m \ \cos \pi h_3 n, \\ Q_x^{\mathrm{FeFe}}(\mathbf{h}) &= 2\pi \sum_{lmn} (c_{\mathrm{Fe}}/c_{\mathrm{Pt}} + \alpha_{lmn}) \langle x_{lmn}^{\mathrm{FeFe}} \rangle \\ &\quad \times \sin \pi h_1 l \ \cos \pi h_2 m \ \cos \pi h_3 n. \end{aligned} \tag{2}$$

Here, $\mathbf{h} = (h_1, h_2, h_3)$, α_{lmn} are the Warren-Cowley short-range order parameters for any neighboring shell lmn, c_μ are the atomic fractions of component μ = Fe, Pt, and $\langle x_{lmn}^{\mu\mu} \rangle$ are the averaged static atomic displacements between μ-μ pairs in units of the lattice parameter a. Furthermore, $\eta = \mathrm{Re}\{f_{\mathrm{Pt}}/[f_{\mathrm{Pt}} - f_{\mathrm{Fe}}]\}$ and $\xi = \mathrm{Re}\{f_{\mathrm{Fe}}/[f_{\mathrm{Pt}} - f_{\mathrm{Fe}}]\}$ are scattering factor ratios. To determine the Fourier coefficients α_{lmn} and $\langle x_{lmn}^{\mu\mu} \rangle$, the Georgopoulos-Cohen (GC) method [27] was employed.

B. Atomistic, magnetic, and electronic-structure modeling

Statistical modeling of magnetic and atomic alloy configurations at finite temperatures has been done using classical Heisenberg and Ising Hamiltonians. In particular, the Heisenberg Hamiltonian had the following form:

$$H^{\mathrm{Heis}} = -\sum_p J_p \sum_{i,j \in p} \mathbf{e}_i \cdot \mathbf{e}_j c_i c_j, \tag{3}$$

where J_p is the magnetic exchange interaction between Fe atoms at coordination shell p in some particular atomic and *magnetic* configuration, $\mathbf{e}_i$ is the unit vector describing the direction of the local magnetic moment at site i, and c_i is the concentration variable taking on values 1 and 0 if site i is occupied by Fe and Pt, respectively. In general, one also adds terms which account for relativistic effects, such as magnetic anisotropy. However, they have been disregarded here due to

their minor contribution to the stability of the magnetic state and the transition temperatures.

The atomic configurational Hamiltonian had the usual Ising form

$$H = \frac{1}{2}\sum_{p} V_p^{(2)} \sum_{i,j\in p} \delta c_i \delta c_j + \frac{1}{3}\sum_{t} V_t^{(3)} \sum_{i,j,k\in t} \delta c_i \delta c_j \delta c_k + \frac{1}{4}\sum_{q} V_q^{(4)} \sum_{ijk\ell\in q} \delta c_i \delta c_j \delta c_k \delta c_\ell \ . \quad (4)$$

Here, δc_i is the concentration fluctuation at site i: $\delta c_i = c_i - c$; $V_s^{(n)}$ is the n-site effective interaction parameter of the cluster (ECI) of an s-type, which depends on the concentration of Fe, the lattice constant of the alloy, and the magnetic state. These ECI parameters are implicitly temperature dependent in quite a complicated way since the magnetic state depends on the alloy configuration and the magnetic interactions, which also determine the magnetic state and in turn depend on the alloy configuration and the magnetic state.

Although the ECI parameters in magnetic systems depend on the local atomic configuration, such a dependence is small in the paramagnetic state and can be neglected. The magnetic transition in Fe_3Pt occurs at quite a low temperature where atomic diffusion is very slow, i.e., all the important and interesting configurational effects occur in the paramagnetic state. Thus, such a configurational dependence was disregarded in this work.

The ECI parameters have been obtained in the random atomic configuration using the screened generalized perturbation method (SGPM) [28,29] implemented in the Green's function exact muffin-tin orbitals (EMTO) technique [30–32]. The coherent potential approximation (CPA) [33,34] has been used in the electronic-structure calculations of random alloys. Screening parameters have been determined in the 864-atom supercell calculations of random Fe-25 at.% Pd in both ferromagnetic and paramagnetic states using the locally self-consistent Green's function (LSGF) method [35]. The paramagnetic state has been modeled by the disordered local moment (DLM) spin configuration [36,37].

The local density approximation [38] has been used for the exchange-correlation potential in the DFT self-consistent calculations, while the total energy has been calculated in the generalized gradient approximation (GGA) [39]. All the EMTO-CPA calculations were performed using an orbital momentum cutoff of $l_{\max} = 3$ for partial waves. Some calculations of the magnetic and chemical interactions have been done by the fully relativistic EMTO-CPA method, which solves the four-component Dirac equation [40].

To account for the local lattice relaxations in the statistical model [Eq. (4)], strain-induced interactions have been calculated in the dilute limit of Pt in Fe using the Kanzaki-Krivoglaz model [41,42]. Forces and atomic displacements were obtained in the projector-augmented-wave (PAW) [43,44] method using the Vienna *ab initio* simulation package (VASP) [45,46]. For that purpose, a 256-atom supercell was produced by a $4 \times 4 \times 4$ repetition of the initial cubic 4-atom supercell.

The PAW-VASP method has also been used to determine static atomic displacements in random and short-range ordered Fe-25 at.% Pt. All the PAW-VASP calculations have been performed using the Perdew-Burke-Ernzerhof (PBE) form for the GGA [39]. The plane-wave energy cutoff was 350 eV. The convergence criteria were 10^{-5} eV for the total energy and 10^{-2} eV/Å for the forces. The integration over the Brillouin zone in the electronic-structure calculations was done using a $4 \times 4 \times 4$ Monkhorst-Pack k-point grid [47].

III. EXPERIMENT

A single crystal with a nominal composition of Fe-27 at.% Pt was produced with 99.95% pure iron from PRAXAIR MRC SA (Meyrin, Switzerland) and 99.95% pure platinum from Johnson Matthey (Zurich, Switzerland). The raw material was alloyed by arc melting in an Ar atmosphere and swaged to a rod. A single crystal was then grown by the Bridgman method.

Two samples, both with a thickness of 3 mm and a diameter of about 11 mm, were cut from the crystal by spark erosion. One sample had a ⟨210⟩ surface normal and was used to measure the diffuse scattering at room temperature and at 427 K. The other sample had a ⟨110⟩ surface normal. It served for the diffuse scattering under a magnetic field H of about 11 kOe that was set up along the in-plane ⟨110⟩ easy axis of magnetization [48,49]. X-ray fluorescence analysis with polycrystalline standards yielded a concentration of Fe-27.1(4) at.% Pt for both samples.

A state of thermodynamic equilibrium was set up for both samples by homogenizing at 1373 K for 2 days and annealing for 6 days at 1123 K before quenching in ice brine. According to Osaka *et al.* [50], a relaxation time of several minutes is expected at 1123 K which is sufficiently short to attain thermal equilibrium by annealing but also higher than the quenching time, by at least one order of magnitude. Following these heat treatments, the surface preparation of both samples was done on a Logitech PM5 precision lapping and polishing system (FIRST, ETH Zurich) up to a grain size of 0.04 μm.

Mo K_α radiation from a 12-kW rotating anode by Rigaku was employed (for details see Ref. [51]). All three diffuse scattering experiments were performed on a three-dimensional grid in reciprocal space with spacings of 0.1 reciprocal lattice units (rlu) and scattering vectors ranging from about 1.5 to 7.0 rlu. For both measurements at room temperature, an additional grid around the X position within a distance of 0.4 rlu [with same spacing, but shifted by (0.05, 0.05, 0.05)] was employed. On the average, about 14 000 positions were taken per scattering experiment.

Data were calibrated using polystyrene. Compton scattering and thermal diffuse scattering up to third order were calculated and subtracted from the calibrated scattering to obtain elastic diffuse scattering. To calculate thermal diffuse scattering and to determine the total (static and dynamical) Debye-Waller factor, elastic constants have to be known. They were determined at room temperature by the pulse-echo-overlap method using a cylinder with a ⟨110⟩ axis and following the same heat treatment. Values of $c_{11} = 125(2)$ GPa, $c_{12} = 91(1)$ GPa, and $c_{44} = 84(1)$ GPa were obtained. These values agree within 8% with the findings of Hausch [52], the difference is believed to be largely due to a high sensitivity of the elastic data

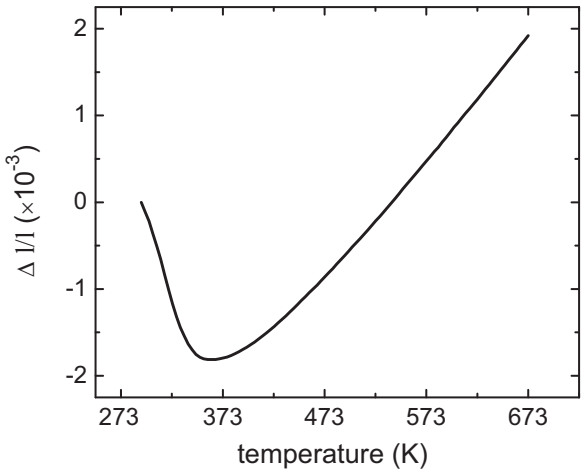

FIG. 1. Macroscopic length change $\Delta l/l$ of Fe-27.1 at.% Pt around the Curie temperature.

on the actual state of order and to the difference of sample composition.

For the two other diffuse scattering experiments, values were taken from Hausch [52]: (i) $c_{11} = 182$ GPa, $c_{12} = 122$ GPa, $c_{44} = 93.8$ GPa at 427 K and (ii) $c_{11} = 122$ GPa, $c_{12} = 88$ GPa, $c_{44} = 87$ GPa under magnetic saturation at room temperature. Finally, atomic scattering factors and Compton scattering values were taken from Ref. [53] and the Hönl corrections from Sasaki [54].

The investigation of the Invar effect on an atomic level was accompanied with dilatometry. An oligocrystalline rod with a diameter of 2.5 mm and a length of 10 mm was measured on a dilatometer type 805A/D (Bähr Thermoanalyse GmbH) with the same thermal history as the samples for diffuse scattering. Figure 1 shows the relative change in length in dependence of temperature with a negative slope around the Curie temperature of ∼360 K (Invar region) and a steady increase at higher temperatures following the Grüneisen relation.

IV. RESULTS FROM SCATTERING

To illustrate the experimental (elastic and inelastic) diffuse scattering of Fe-27.1 at.% Pt, the pattern for the (100) plane is shown in Fig. 2. The measurement at room temperature was chosen; the patterns for the measurements at 427 K and under magnetic field are barely distinguishable. One always notes strong diffuse maxima of up to ∼10 Lu at 100 positions, i.e., at the $L1_2$ superstructure positions of the ordered Fe_3Pt phase. The diffuse maxima show no shift from the exact X position, only a slight asymmetry along ⟨100⟩ is seen in the surrounding pattern. Both findings imply that the displacement scattering is much lower than short-range order scattering within the selected range of scattering vectors.

After subtraction of thermal diffuse scattering and Compton scattering, the elastic diffuse scattering was analyzed using the method of Georgopoulos and Cohen [27]. The underlying Fourier series of short-range order scattering and linear displacement scattering were then least-squares fitted to obtain the Warren-Cowley short-range order parameters α_{lmn} and

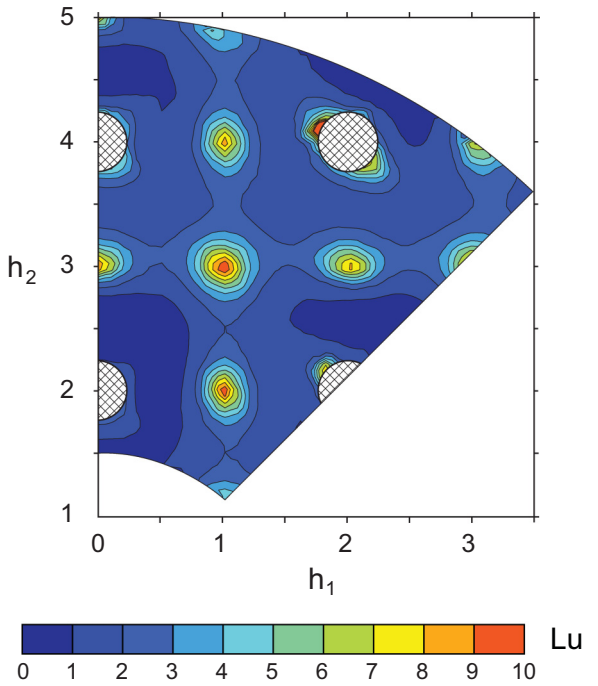

FIG. 2. (Color online) As-measured diffuse scattering of Fe-27.1 at.% Pt at RT in Lu. The hatched areas around Bragg reflections present the regions that were not employed in data evaluation due to strong thermal diffuse scattering.

the species-dependent static atomic displacements $\langle x^{\mu\mu}_{lmn}\rangle$. The number of relevant parameter sets was determined by considering the R value of the fits, the magnitude of the standard deviations with respect to those of the Fourier coefficients, and a comparison of the separated and recalculated short-range order scattering and displacement scattering, respectively.

A. Short-range order

The separated short-range order scattering for all three states is shown in Fig. 3. Around the maxima at 100 the lines of equal intensity have a disklike shape. Such a pattern is well known to arise from configurations when diffuse antiphase boundaries of conservative nature are present, like, e.g. in Cu-25 at.% Au (Ref. [55]) or Ni-25 at.% Pt (Ref. [56]).

Due to the strong modulation in scattering 40 α_{lmn} are required to reproduce the maximum in intensity at X position. The leading parameters are given in Table I; the standard deviations are exclusively based on counting statistics. A close agreement among all three states is found: the standard deviation among the three data sets σ amounts (on the average) to only 0.9 σ for each individual parameter. The largest spread among parameters is seen in α_{000} where it is 4 σ. A close agreement among the three states is expected, as the temperature range of the measurements is sufficiently low to avoid any distinct ordering.

The experimental value of α_{000} is lower than the theoretical value of 1. Such deviations are repeatedly seen in literature and reflect uncertainties not stemming from counting statistics, but from calibration, determination of the inelastic scattering contributions, or separation into the different elastic scattering

TABLE I. Warren-Cowley short-range order parameters of Fe-27.1 at.% Pt at room temperature, at 427 K, and at RT under magnetic saturation as determined from x-ray diffuse scattering. Data of the first 21 shells are shown. Theoretical results are at 1320 K, which is 80 K above the theoretical order-disorder transition temperature.

	α_{lmn}			
lmn	RT	427 K	RT Magnetic saturation	Theory, 1320 K
000	0.9593 (70)	0.9010 (65)	0.9302 (81)	1.0
110	−0.1334 (45)	−0.1177 (39)	−0.1312 (47)	−0.120
200	0.1790 (40)	0.1784 (36)	0.1630 (44)	0.185
211	−0.0137 (29)	−0.0066 (25)	−0.0097 (32)	−0.008
220	0.0782 (27)	0.0804 (24)	0.0741 (30)	0.085
310	−0.0448 (19)	−0.0426 (18)	−0.0386 (22)	−0.045
222	0.0454 (21)	0.0454 (20)	0.0441 (25)	0.042
321	−0.0129 (12)	−0.0123 (11)	−0.0136 (15)	−0.016
400	0.0460 (21)	0.0419 (20)	0.0294 (27)	0.052
330	−0.0171 (13)	−0.0171 (13)	−0.0192 (17)	−0.019
411	0.0047 (13)	0.0064 (12)	0.0014 (16)	0.006
420	0.0261 (12)	0.0280 (12)	0.0294 (15)	0.032
233	−0.0074 (10)	−0.0073 (9)	−0.0062 (12)	−0.009
422	0.0190 (10)	0.0190 (10)	0.0171 (13)	0.020
431	0.0008 (8)	−0.0003 (8)	−0.0015 (9)	−0.002
510	−0.0152 (13)	−0.0157 (12)	−0.0101 (15)	−0.018
521	−0.0067 (9)	−0.0080 (8)	−0.0067 (10)	−0.010
440	0.0081 (13)	0.0097 (13)	0.0081 (17)	0.015
433	−0.0000 (10)	−0.0020 (9)	−0.0017 (12)	−0.003
530	−0.0049 (10)	−0.0057 (10)	−0.0038 (13)	−0.009
244	0.0068 (10)	0.0066 (10)	0.0090 (13)	0.011
600	0.0103 (20)	0.0071 (18)	−0.0041 (25)	0.019

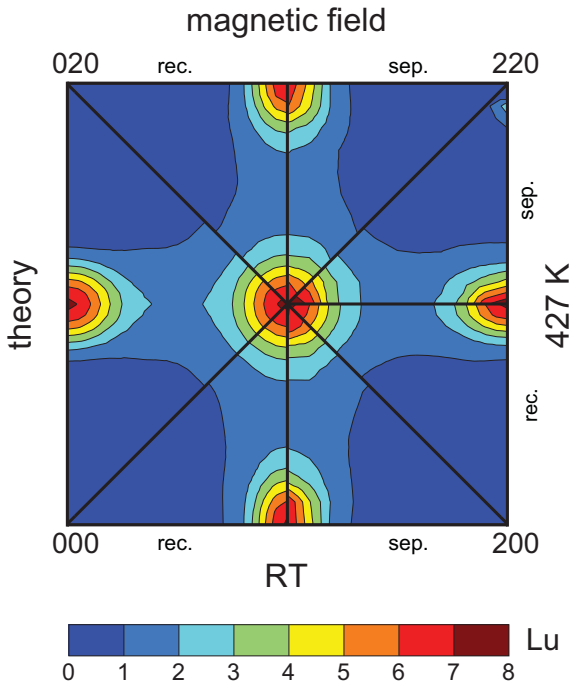

FIG. 3. (Color online) Short-range order scattering I_{SRO} of Fe-27.1 at.% Pt at room temperature, at 427 K, and at RT under saturating magnetic field. The as-separated and as-fitted intensities are shown.

contributions. Consistently with the large scattering intensity at 100, the magnitude of α_{110} amounts to about one third of maximally ordered Fe-27.1 at.% Pt. The sign sequence of the α_{lmn} up to shell 330 is the same as that of the $L1_2$ structure. A difference in sign along with a large value for α_{800} might be connected with the presence of diffuse antiphase boundaries.

B. Static atomic displacements

To fit the static atomic displacements from the Fourier series $\mathbf{Q}^{\mathrm{FeFe}}$ and $\mathbf{Q}^{\mathrm{PtPt}}$, only six neighboring shells can be considered. Otherwise, strong correlations arise among the Fourier coefficients. The static atomic displacements are given in Table II, and the recalculated terms $\mathbf{h} \cdot \mathbf{Q}^{\mu\mu}$ are shown in Fig. 4 for the state at RT under magnetic saturation. Figure 4 illustrates that the two terms $\mathbf{h} \cdot \mathbf{Q}^{\mu\mu}$ contribute with different signs to the total displacement scattering. This is a well-known feature. Still, a build up in modulations (compensated in total scattering) is prohibited by the ridge-regression technique within the Georgopoulos-Cohen method.

The number of static atomic displacements can be largely enhanced if one assumes that the displacement of any neighboring shell may be approximated just by a radial displacement, i.e., without considering cubic symmetry of the alloy. Then, 16 shells turned out to be best suited. The respective values are also given in Table II for those shells that have radial displacements under the lattice symmetry. Good agreement is seen for the strongest nearest-neighbor displacements, and on a slightly reduced level for the next-nearest ones. As a general feature one observes that the displacements among Fe-Fe pairs are smaller than those between Pt-Pt pairs. This is a well-known situation: the majority species (here Fe) mainly determines the average lattice and is thus less subject to displacements from the sites of the average lattice.

Figure 5 (like Table II) reveals a strikingly systematic tendency for the displacements of the first two shells: the magnitude of the atomic displacements increases from the state at 427 K over the one at RT to the one at RT under saturating magnetic field. Thus, spontaneous volume magnetostriction for the two measurements at different temperatures as well as forced volume magnetostriction at fixed temperature act in the same way with respect to the near-field deviations from the average lattice.

C. Effective pair interaction parameters

Based on the Warren-Cowley short-range order parameters, effective pair interaction (EPI) parameters $V_{lmn} = V_{lmn}^{AA} + V_{lmn}^{BB} - 2V_{lmn}^{AB}$ were determined using the inverse Monte Carlo method [57]. The average over the three short-range order (SRO) parameter sets was taken for modeling crystals of $48 \times 48 \times 48$ atoms under linear boundary conditions. The EPI parameters of the Ising Hamiltonian enter the ordering energy per atom, E_{ord}, of an A-B alloy through

$$E_{\mathrm{ord}} = \frac{1}{2} c_A c_B \sum_{lmn} V_{lmn} \alpha_{lmn} \ . \qquad (5)$$

In spite of the averaged SRO parameter set, it still turned out impossible to reproduce the short-range ordered state of the measurements in Monte Carlo simulations, independent of the number of EPI parameters. This deficiency is due to

TABLE II. Species-dependent static atomic displacements of Fe-27.1 at.% Pt at room temperature, at 427 K, and at RT under magnetic saturation, in units of the lattice parameter. In comparison, data are also given when the radial approximation was applied.

Room temperature

lmn	$\langle x_{lmn}^{\mathrm{PtPt}}\rangle$	Radial approx.	$\langle x_{lmn}^{\mathrm{FeFe}}\rangle$	Radial approx.	$\langle x_{lmn}^{\mathrm{FePt}}\rangle$	Radial approx.
110	0.02511 (11)	0.02574 (8)	0.00297 (1)	0.00276 (1)	−0.00575 (2)	−0.00559 (1)
200	−0.00535 (23)	−0.00781 (20)	−0.00143 (6)	−0.00177 (5)	0.00413 (12)	0.00551 (11)
211	−0.00096 (8)		0.00016 (1)		−0.00003 (2)	
121	−0.00128 (6)		−0.00031 (1)		0.00061 (2)	
220	−0.00170 (8)	−0.00016 (11)	−0.00001 (2)	−0.00015 (3)	0.00043 (3)	0.00025 (5)
310	0.00528 (9)		0.00014 (1)		−0.00099 (2)	
130	0.00114 (10)		−0.00021 (2)		0.00007 (3)	
222	−0.00087 (9)	−0.00072 (7)	−0.00021 (2)	0.00003 (1)	0.00047 (3)	0.00012 (2)

427 K

lmn	$\langle x_{lmn}^{\mathrm{PtPt}}\rangle$	Radial approx.	$\langle x_{lmn}^{\mathrm{FeFe}}\rangle$	Radial approx.	$\langle x_{lmn}^{\mathrm{FePt}}\rangle$	Radial approx.
110	0.02237 (11)	0.02295 (8)	0.00194 (2)	0.00195 (1)	−0.00461 (2)	−0.00469 (1)
200	−0.00196 (25)	−0.00374 (20)	0.00004 (7)	0.00037 (4)	0.00059 (14)	0.00065 (9)
211	−0.00214 (8)		−0.00053 (2)		0.00105 (3)	
121	−0.00111 (6)		−0.00029 (1)		0.00056 (2)	
220	−0.00213 (8)	−0.00084 (11)	−0.00023 (2)	−0.00060 (2)	0.00085 (3)	0.00105 (4)
310	0.00550 (9)		−0.00022 (2)		−0.00061 (3)	
130	0.00173 (10)		−0.00002 (2)		−0.00025 (3)	
222	−0.00112 (9)	−0.00158 (7)	−0.00022 (2)	−0.00019 (1)	0.00054 (3)	0.00060 (2)

RT, magnetic saturation

lmn	$\langle x_{lmn}^{\mathrm{PtPt}}\rangle$	Radial approx.	$\langle x_{lmn}^{\mathrm{FeFe}}\rangle$	Radial approx.	$\langle x_{lmn}^{\mathrm{FePt}}\rangle$	Radial approx.
110	0.03173 (10)	0.03201 (8)	0.00475 (2)	0.00459 (2)	−0.00836 (2)	−0.00822 (2)
200	−0.00888 (22)	−0.00950 (21)	−0.00198 (10)	−0.00133 (9)	0.00599 (17)	0.00515 (16)
211	0.00011 (8)		0.00005 (3)		−0.00008 (4)	
121	−0.00101 (6)		−0.00037 (2)		0.00064 (3)	
220	−0.00140 (8)	0.00031 (11)	−0.00020 (2)	0.00011 (4)	0.00062 (3)	−0.00023 (6)
310	0.00595 (9)		0.00085 (2)		−0.00196 (3)	
130	0.00040 (9)		−0.00006 (2)		0.00001 (3)	
222	−0.00090 (9)	−0.00082 (7)	−0.00026 (3)	−0.00001 (3)	0.00054 (4)	0.00019 (4)

the proximity of the aging temperature (1123 K) to the order-disorder transition temperature (1043 K, see Ref. [50]; earlier the transition temperature was given as 1093 K according to Ref. [58]). Considering the magnitude and the standard deviations of the V_{lmn}, 21 shells were finally employed. Table III gives the EPI set. The uncertainties were obtained by using six sets of SRO parameters, compatible with the normal distribution of the α_{lmn}. Subsequent Monte Carlo simulations yielded an order-disorder transition temperature of 1088(10) K, in excellent agreement with those from direct experimental findings.

V. FIRST-PRINCIPLES RESULTS

A. Magnetic interactions in Fe-rich Fe-Pt alloys

In Sec. II B, it has been mentioned that magnetic interactions in Fe-Pt depend on the alloy composition, lattice constant, magnetic state, and in fact on the atomic configurational state. Figure 6 shows the concentration dependence of the nearest-neighbor magnetic exchange interactions, which have been calculated at a fixed lattice constant of 3.75 Å, a value that corresponds approximately to the experimental lattice constant of random Fe-27 at.% Pt. [14,59]. In this figure, the interactions at the first coordination shell of the fcc lattice are shown in the ferromagnetic (FM) and DLM (paramagnetic) states. Also shown are the interactions in the DLM state in $L1_2$ ordered Fe_3Pt.

Apart from a pronounced concentration dependence, the nearest-neighbor exchange interaction J_{xc} exhibits also quite a strong dependence on the magnetic state for Fe-rich Fe-Pt. In the FM state, this exchange interaction is much stronger than in the DLM state. Basically, this means that a classical Heisenberg Hamiltonian is unable to fully describe the system. The reason for such a dramatic growth of the exchange interactions in the FM state is the substantial increase in the local magnetic moment of Fe in the FM state, which is about 2.6 μ_B, while it is only 2.3 μ_B in the DLM state. Since the magnetic exchange interactions are proportional to the square

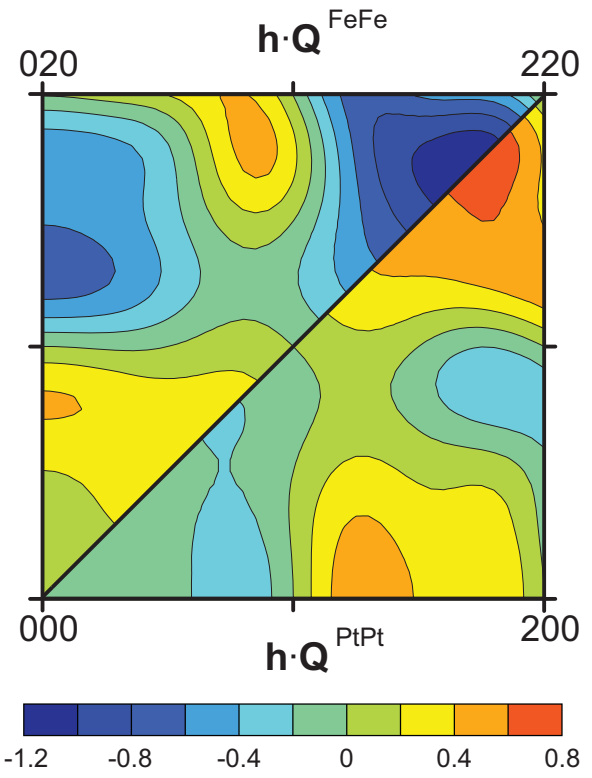

FIG. 4. (Color online) Size-effect scattering $\mathbf{h}\cdot\mathbf{Q}^{\mathrm{FeFe}}$ and $\mathbf{h}\cdot\mathbf{Q}^{\mathrm{PtPt}}$ of Fe-27.1 at.% Pt at RT under saturating magnetic field. The fitted scattering is shown.

of the magnitude of the local magnetic moment, they should be stronger by about 30% in the FM state than in the DLM state.

This strong dependence of the local magnetic moment on the magnetic state in Fe-Pt is the origin of the Invar effect as has been demonstrated in Ref. [5]. The reduction of the magnetization with increasing temperature leads to reduced local magnetic moments of Fe atoms and consequently to the decrease of the equilibrium volume of the alloy, which compensates for the thermal expansion due to anharmonic effects.

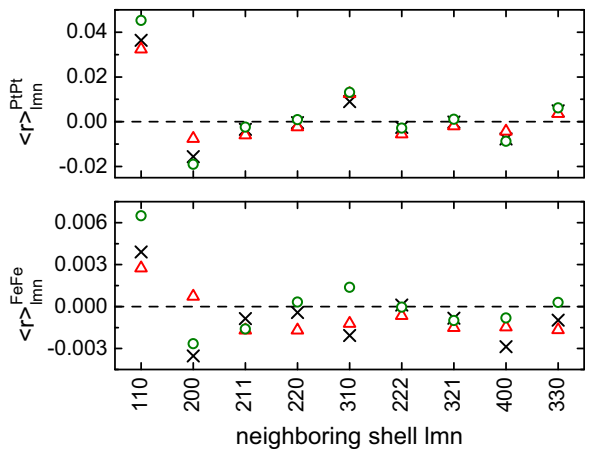

FIG. 5. (Color online) Species-dependent static atomic displacements of Fe-Fe and Pt-Pt pairs in radial approximation. The values in radial direction $\langle r\rangle_{lmn}^{\mu\mu}$ are shown in units of the lattice parameter.

TABLE III. EPI parameters of Fe-27.1 at.% Pt based on the SRO parameters from diffuse scattering.

lmn	V_{lmn} (mRy)
110	6.10 (33)
200	−2.31 (28)
211	−0.08 (9)
220	−0.30 (7)
310	0.28 (8)
222	−0.75 (7)
321	−0.33 (2)
400	0.57 (15)
330	−0.24 (4)
411	−0.05 (5)
420	−0.32 (5)
233	−0.38 (4)
422	−0.23 (3)
431	−0.21 (3)
510	0.13 (8)
521	−0.14 (2)
440	0.01 (1)
433	−0.07 (2)
530	−0.21 (3)
244	−0.07 (3)
600	0.25 (6)

A strong dependence of the nearest-neighbor interaction on concentration is the effect of the filling of the majority d band of Fe. As one can see in Fig. 6, such a dependence is in fact even much more pronounced when the corresponding lattice expansion with concentration is taken into consideration.

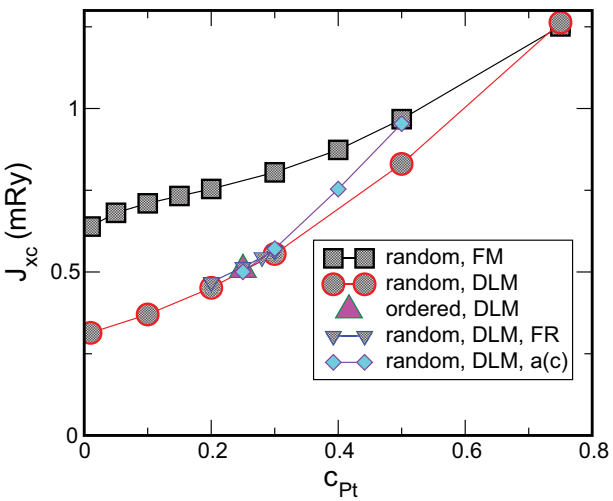

FIG. 6. (Color online) Fe-Fe magnetic exchange interaction J_{xc} at the first coordination shell in Fe-Pt alloys as a function of concentration. All the results but those shown by diamonds are obtained at a fixed lattice constant of 3.75 Å. The results shown by diamonds are obtained at the experimental room-temperature lattice constants. The large up triangle shows the result of the scalar relativistic calculations of the $L1_2$ ordered Fe_3Pt. Only the results shown by squares are obtained in the FM state, all the others in the DLM state. Small down triangles show the results of the fully relativistic calculations, which include spin-orbit coupling.

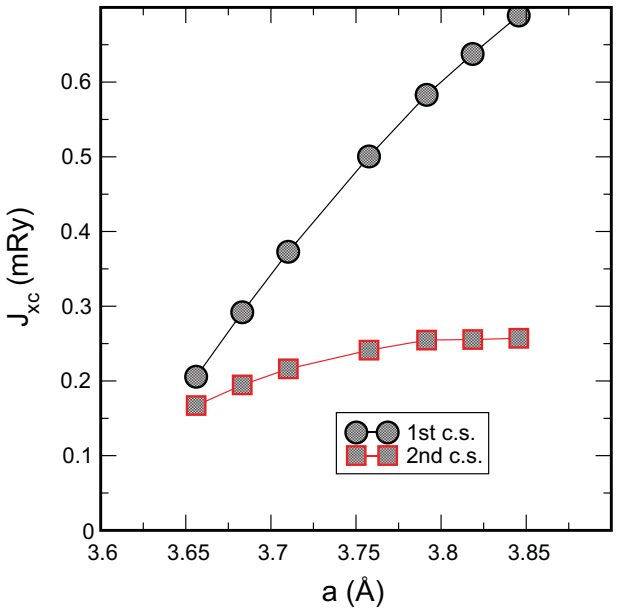

FIG. 7. (Color online) Fe-Fe magnetic exchange interactions at the first two coordination shells in random Fe-25 at.% Pt as function of the lattice constant in the DLM state.

Figure 7 shows the dependence of the magnetic exchange interactions at the first two coordination shells on the lattice constant in random Fe-25 at.% Pt in the DLM state. Obviously, the lattice parameter plays an important role in the magnetic interactions of Fe atoms, which explains the strong pressure dependence of the Curie temperature in Fe-rich Fe-Pt alloys [60].

Figure 8 shows the magnetic exchange interactions at close-by coordination shells in random and $L1_2$ ordered Fe-25 at.% Pt in the DLM state. One can see that the

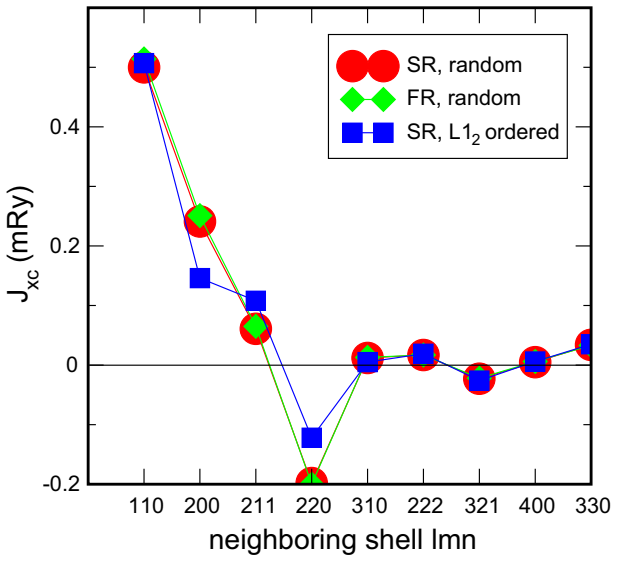

FIG. 8. (Color online) Fe-Fe magnetic exchange interactions in the DLM state in random Fe-25 at.% Pt, obtained in the scalar (SR) and fully relativistic (FR) calculations and in $L1_2$ ordered Fe_3Pt for the same lattice constant of 3.75 Å.

atomic configuration mainly affects the magnetic exchange interactions at the second, third, and fourth coordination shells. In order to demonstrate that this is quite a substantial effect, we calculated the Curie temperature using these interactions and found that the magnetic interactions for random Fe-25 at.% Pt yield a substantially lower Curie temperature (about 290 K) than those for the $L1_2$ ordered Fe_3Pt (about 450 K). This means that for the correct description of the magnetic phase transition in Fe-Pt alloys, one should use magnetic exchange interaction parameters determined for the corresponding configurational state [61].

It is experimentally well established that the Curie temperature in Fe-rich Fe-Pt alloys depends on the state of the atomic order: It is higher in the ordered than in the random state, by about 150 K [15,62]. This can be the result of two factors: (i) the effect of atomic order itself due to different atomic distribution functions at each coordination shell and (ii) the effect of atomic order on the magnetic exchange interactions, which has been demonstrated above. In order to investigate the first effect, we have calculated the Curie temperature in the $L1_2$ ordered Fe_3Pt alloy using magnetic exchange interactions of the ordered phase and found that the Curie temperature drops to 380 K from 450 K (case of random Fe-25 at.% Pt, see above).

In other words, for a fixed set of exchange interaction parameters in Fe-rich Fe-Pt alloys, atomic ordering towards $L1_2$ leads to a *decrease* of the magnetic transition temperature. In the single-site mean-field approximation, the respective change of the Curie temperature in the $L1_2$ ordered phase relative to that in a random alloy is proportional to

$$\Delta T_c \propto \tfrac{1}{3}\left\{-\tfrac{12}{3}J_{110} + 6J_{200} - \tfrac{24}{3}J_{211} + 12J_{220} + \cdots\right\}, \qquad (6)$$

which is negative for a fixed set of exchange interactions either in random or ordered alloy configuration. Therefore, the experimentally observed *increase* of the Curie temperature with increasing atomic order is the effect of the renormalization of the exchange interactions due to atomic order.

Let us note that the existing experimental data for the Curie temperature in Fe_3Pt are somewhat higher than the theoretical result for the completely ordered phase in the scalar relativistic approximation (380 K). According to Ref. [62], the transition temperature in $L1_2$ ordered Fe_3Pt is about 420 K, while it is about 270 K in random Fe-25 at.% Pt. In another experimental study [48], the transition temperature in the ordered Fe_3Pt is 421 and 447 K for a partially ordered alloy with a long-range order parameter of 0.76 and 1, respectively.

Nevertheless, the agreement is reasonable and can be further improved. First of all, theoretical magnetic exchange interactions are obtained in the DLM state, which is closer to the magnetic state at the Curie temperature (zero or very small magnetization) than the completely ordered FM state. In fact, one could account for magnetic short-range order, which is substantial at the Curie temperature, and this should increase the strongest interaction at the first coordination shell (see Fig. 6) and therefore the Curie temperature. Second, it is important to account for the thermal expansion at 450 K, where the experimental phase transition is observed, and this should also lead to an increase of the Curie temperature. And,

finally, a non-negligible contribution can come from Pt atoms, which may acquire nonzero magnetic moment both due to influence of Fe atoms and thermally induced longitudinal spin fluctuations.

This means that consistent theoretical calculations of the Curie temperature in these alloys should be done in a self-consistent manner even for a fixed atomic configuration, where the magnetic exchange interactions are renormalized according to the change of the temperature and the magnetic state. However, such an exercise is beyond the scope of the paper. In the end, it will of course lead to quantitative changes, which might bring the calculated Curie temperature to perfect agreement with experimental data. However, this proves nothing about the theory, which still will remain quite approximate due to other approximations involved in the calculations, starting from the one for the exchange-correlation energy.

The important message here is that magnetic interactions in Fe-rich Fe-Pt alloys depend on all possible external and internal parameters, such as the atomic and magnetic configurational states. This fact has very important consequences for the proper theoretical modeling of thermodynamics of Fe-Pt alloys, basically meaning that the usual cluster expansions done for enthalpies of formation in the ferromagnetic state can be in large error for finite-temperature thermodynamics.

B. Effective chemical interactions

Effective chemical interactions have been calculated by the SGPM method for random Fe-Pt alloys in both FM and DLM states. In the case of magnetic alloys, chemical interactions can in fact quite strongly depend on alloy configuration [63]. These effects, however, will be neglected since an accurate quantitative description of the finite-temperature thermodynamics of this system is very complicated due to nontrivial magnetism and large atomic size mismatch of the alloy components.

First, the concentration and magnetic state dependence of the ECI parameters is demonstrated. Figure 9 shows the concentration dependence of the chemical part of the nearest-neighbor ECI parameters $V_1^{(2)}$ obtained in the FM and DLM states. The calculations have been done for a fixed lattice constant of 3.75 Å in order to separate volume effects.

Part of the difference between the interactions in the FM and DLM states can be associated with the corresponding magnetic exchange interactions [64,65]. Since the magnetic exchange interaction at the first coordination shell is of the ferromagnetic type (and the magnetic Fe-Fe interaction is more attractive in the FM state), the FM effective chemical interaction is less positive than that in the DLM state. The concentration dependence of the FM and DLM ECI parameters $V_1^{(2)}$ somewhat differs, especially for Fe-rich alloy compositions, which is most probably related to some electronic effects associated with the change of the Fermi surface topology in this region [63].

In this case, one can expect strong sensitivity of the many-atom interactions in the corresponding concentration interval. Indeed, one can see in Fig. 10 that the concentration dependence of the higher-order three- and four-site interactions is not less pronounced than that of the pair interactions.

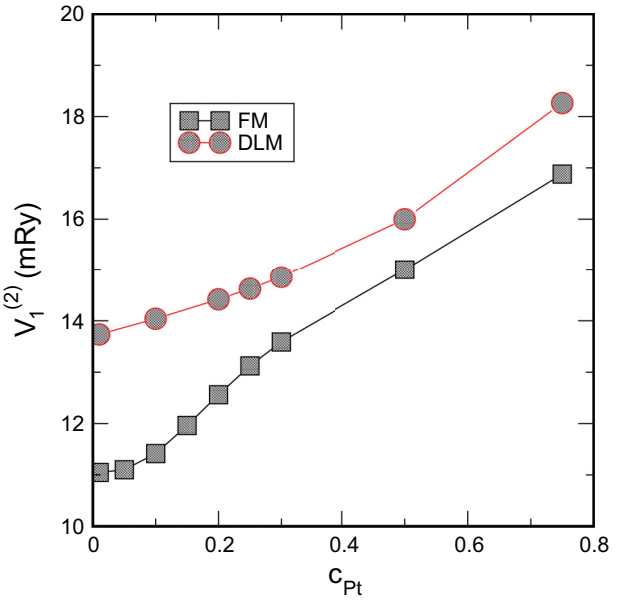

FIG. 9. (Color online) Effective pair chemical interactions (chemical part from SGPM calculations) at the first coordination shell in random Fe-Pt alloys as function of Pt concentration.

In this figure, two three-site interactions are shown: $V_{111}^{(3)}$ for the triangle of nearest neighbors and $V_{411}^{(3)}$ for the cluster of three subsequent sites on the line in the closed-packed direction [110], and two four-site interactions: $V_1^{(4)}$ for the tetrahedron of nearest neighbors and $V_4^{(4)}$ for the cluster of four subsequent sites on the line in the closed-packed direction. One notices that the interactions in the FM state exhibit quite a nonlinear

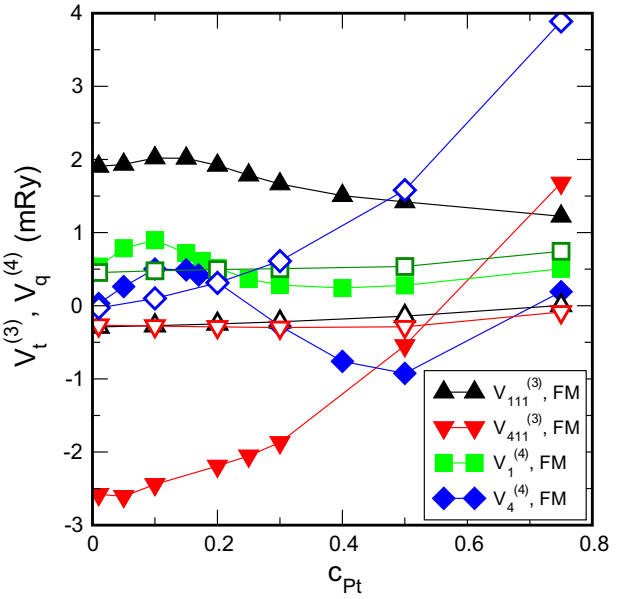

FIG. 10. (Color online) Effective three-site $V_t^{(3)}$ and four-site $V_q^{(4)}$ chemical interactions in random Fe-Pt alloys as function of Pt concentration. Filled symbols show the interactions in the FM state, while the corresponding open symbols show the interactions in the DLM state.

concentration behavior, which becomes more pronounced with increasing order of the interactions.

C. ECI parameters and statistical simulations for Fe-27 at.% Pt

One of the most serious complications in a first-principles description of effective interactions in the Fe-Pt system is the substantial size mismatch of its alloy components. Partly, this is the reason for a quite strong ordering tendency due to electrostatic effects. On the other hand, the ordering tendency at the first coordination shell is compensated by the strong strain-induced interaction, which is attractive for alloy components of the same type.

Unfortunately, a strict first-principles description of the strain-induced interactions is possible only in the dilute limit of one component in the other. This creates a problem in our case since fcc Fe is a mechanically unstable system in the FM state, at least within the range of Fe-rich Fe-Pt alloys lattice constants. The other problem is that it is quite difficult to do calculations in the paramagnetic state, which is relevant at the temperatures of the order-disorder phase transition in Fe-27 at.% Pt.

Therefore, we have estimated the strongest strain-induced interactions using a harmonic superposition model [66], assuming that local atomic displacements are small and thereby only the harmonic contribution is important. In this case, the force acting on a host atom due to two impurity atoms and the resulting displacements are given by a superposition of the forces and displacements produced by each impurity atom. Thus, using the Hellmann-Feynman forces from the first-principles calculations of the host atoms around a *single* impurity $\mathbf{F}_i$ (before relaxation), and local displacements of the host atoms $\mathbf{u}_i$ (after relaxation), one can determine the strain-induced interactions as

$$V^{\mathrm{si}}(\mathbf{R}_p) = -\frac{1}{2}\sum_i \left[\left(\mathbf{F}_i^1 + \mathbf{F}_i^2\right)\left(\mathbf{u}_i^1 + \mathbf{u}_i^2\right) - \mathbf{F}_i^1\mathbf{u}_i^1 - \mathbf{F}_i^2\mathbf{u}_i^2\right]. \tag{7}$$

Here, the summation is performed over all host atoms, and $\mathbf{F}_i^{1(2)}$ and $\mathbf{u}_i^{1(2)}$ are the forces and displacements induced either by the first (1) or second (2) impurity atom, respectively, with $\mathbf{R}_p$ being their distance vector. This model is in fact equivalent to the widely used Krivoglaz-Kanzaki model [41,42,67].

In this work, we have used a 256-atom supercell containing 255 Fe atoms and a single Pt atom to determine the static lattice displacements $\mathbf{u}_i$ and the Kanzaki forces $\mathbf{F}_i$ caused by the presence of the Pt atom. The calculations have been done in the FM state.

In Fig. 11, we show the calculated chemical and total interactions, which were determined as

$$V_p^{(2)} = V_p^{(2)-\mathrm{ch}} + V^{\mathrm{si}}(\mathbf{R}_p) \tag{8}$$

at the first three coordination shells where the strain-induced interactions are the strongest. The strain-induced interactions are in fact quite long ranging. However, there is large uncertainty as Eq. (8) has been used in the wrong magnetic state and the dilute limit was assumed. At the same time, the magnetic state affects the magnitude of the local magnetic moment and thus the effective size of Fe and Pt atoms. The chemical ECI parameters of random Fe-27 at.% Pt have been calculated at 1200 K, using a lattice constant of 3.79 Å as

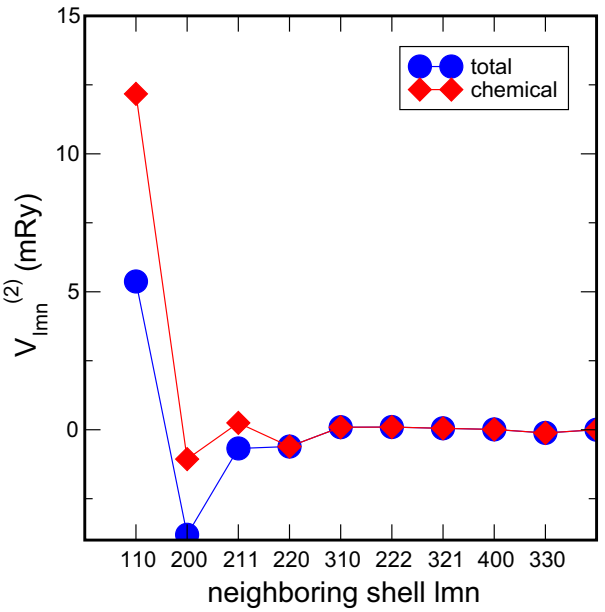

FIG. 11. (Color online) Total and chemical ECI parameters $V_{lmn}^{(2)}$ in random Fe-27 at.% Pt. The chemical interactions are calculated in the DLM state at a lattice constant of 3.79 Å.

estimated in the Debye-Grüneisen model. The calculations have been done in the DLM state.

There are several quite strong three- and four-site interactions, the strongest among them were presented in Fig. 10. These interactions in the DLM state together with the ECI parameters given in Fig. 11 have been used in the Monte Carlo simulations of Fe-27 at.% Pt. The order-disorder transition temperature is 1240 K, which is about 200 K higher than the experimental value. The theoretical atomic SRO parameters at 1320 K which is 80 K above the order-disorder phase transition, was compared with those from diffuse scattering that were taken from a state also about 80 K above the experimental order-disorder transition temperature. Table I shows that the agreement between theoretical and experimental results is very good in the SRO parameters, and also in the contour plot of Fig. 3.

D. Static lattice displacements in Fe-25 at.% Pt

Theoretical investigations of atomic displacements in Fe-25 at.% Pt with and without atomic SRO have been performed using a 256-atom supercell. Calculations have been done for two atomic configurations: The first with $\alpha_{lmn} = 0$ up to the eighth coordination shell, the other with the following SRO parameters at the first six coordination shells: $\alpha_{1-6} = -0.125, 0.167, -0.007, 0.055, -0.046, 0.016$. The latter parameter set corresponds to the high-temperature state of the alloy just above the order-disorder phase transition and, in particular, this alloy configuration is close to the one used in the experiment.

The PAW first-principles calculations have been done by VASP in the FM state. Unfortunately, the *ab initio* modeling of the paramagnetic state with a reduced magnetization is practically impossible for such a large supercell. On the other hand, the modeling of lattice displacements on a smaller unit

TABLE IV. Static atomic displacements of Fe-25 at.% Pt without and with atomic SRO determined from first-principles calculations of a 256-atom supercell in the FM state. Values (in radial approximation) are given in units of the lattice parameter.

lmn	$\langle x_{lmn}^{\mathrm{PtPt}}\rangle$	$\langle x_{lmn}^{\mathrm{FeFe}}\rangle$	$\langle x_{lmn}^{\mathrm{FePt}}\rangle$
	Random alloy		
110	0.0363	−0.0060	0.0029
200	0.0001	−0.0024	0.0035
211	0.0049	−0.0014	0.0013
220	0.0048	−0.0013	0.0012
	With atomic SRO		
110	0.0275	−0.0037	0.0022
200	−0.0067	−0.0023	0.0063
211	0.0016	0.0003	−0.0007
220	0.0008	−0.0007	0.0009

cell does not make much sense: even in the case of a 256-atom supercell, the meaningful results are restricted to just a few nearest-neighbor coordination shells. Theoretical results are presented in Table IV.

One can see that there is a pronounced effect of the atomic SRO upon the lattice displacements: the Pt-Pt interatomic distances appear to be reduced while Fe-Fe distances are increased in the alloy with atomic SRO relative to those in the completely random alloy. The theoretical results with atomic SRO can be compared with the experiment done with saturating magnetic field. Although the agreement is not perfect, it is much better than between theoretical results without SRO. In other words, experiment and theory indicate that atomic displacements are sensitive to the atomic configuration and the magnetic state.

VI. DISCUSSION

In general, static atomic displacements are more difficult to be determined from diffuse scattering than short-range order parameters. The reason for this is that there are up to six unknowns per neighboring shell with $\langle x_{lmn}^{\mu\mu}\rangle$ instead of just one unknown as with α_{lmn}. Two approaches may be employed to determine these parameters for concentrated solid solutions: the Georgopoulos-Cohen method [27] and the 3λ method [9]. A prerequisite of the 3λ method is that elements in the alloy are nearby in the periodic table, in which case the Georgopoulos-Cohen method at a laboratory x-ray source is doomed to fail due to missing scattering contrast. Thus, this method is not applicable with Fe-Pt.

In two cases, Fe-Cr and Ni-Cr, a comparison of both evaluation procedures was done using data taken at well-chosen x-ray energies at a storage ring to reach a good scattering contrast: excellent agreement in $\langle x_{lmn}^{\mu\mu}\rangle$ was achieved with Fe-Cr (Ref. [24]) with both methods and to a somewhat minor degree with Ni-Cr (Ref. [69]). The pros and cons of both approaches are only partly settled if one employs neutrons in comparison as access to a linear combination of the species-dependent static atomic displacements is then provided: values may nicely agree when one determines them from the species-dependent displacements as with, e.g., Ni-Al (Ref. [70]), still there might be an improper separation of *A*-*A* and *B*-*B* displacement scattering of the *A*-*B* alloy. A procedure to reduce the number of displacement parameters consists in employing the radial approximation. Table II shows that this assumption is doubtful. For example, it is certainly not fulfilled when the two atomic displacement parameters of a shell differ in sign. Further points on the displacement parameters in Fe-Pt might be noted.

(i) For the separation of species-dependent static atomic displacements by the Georgopoulos-Cohen method, several requirements have to be fulfilled: a largely different variation of the scattering factor ratios η and ξ with scattering vector (here by 20%) and also a high scattering contrast (here $\Delta Z = 52$, Z = atomic number), and good counting statistics at a large number of symmetry-equivalent positions (∼90 positions). Still, to test whether the size effect scattering $I_{\mathrm{SE}}(\mathbf{h})$ is well separated within the elastic diffuse scattering, a Borie-Sparks (BS) analysis [71] may be applied. Here, one deliberately discards the difference in η and ξ with scattering vector. Such an approach may then serve as an indicator for the separation as much less (10 instead of 25) Fourier series have to be considered. The linear combination of the species-dependent static atomic displacements of the BS analysis was compared with the one using Table II and scattering factor ratios η and ξ that are averaged over the range of scattering vectors. With $\gamma_{x,lmn}^{\mu\mu}$ being the Fourier coefficients of the Fourier series of Eq. (2) and

$$\gamma_{x,lmn} = \eta\gamma_{x,lmn}^{\mathrm{PtPt}} + \xi\gamma_{x,lmn}^{\mathrm{FeFe}} \tag{9}$$

one obtains −0.0377(2) and −0.242(23) for the 110 shell, and 0.0278(12) and 0.0373(73) for the 200 shell (first value is based on the GC, the second comes from the BS analysis). One notes that comparable data are obtained.

(ii) EXAFS measurements also provide species-dependent near-neighbor distances. Investigations done by Maruyama *et al.* [72] give values at 300 K for disordered Fe-Pt foils with 26 and 28 at.% Pt quenched from 1073 K and thus allow of an interpolation to the present composition of Fe-27.1 at.% Pt. Using the lattice parameter of the present investigation at RT [$a = 3.7507(28)$ Å], one obtains $\langle x_{110}^{\mathrm{PtPt}}\rangle = 0.0180(14)$ and $\langle x_{110}^{\mathrm{FePt}}\rangle = -0.0050(14)$. Both values are close to 0.02511(11) and −0.00575(2), respectively, of Table II.

(iii) Local lattice displacements as well as Kanzaki forces are usually quite well reproduced in first-principles calculations since they are related to small structural perturbations, where large errors of the exchange-correlation functionals are quite well compensated (canceled). In the present investigation, general agreement is found between theory and experiment on the magnitude of the static atomic displacements. Still, there is one clear difference that refers to the sign of the nearest-neighbor displacement of Fe-Fe and Fe-Pt pairs. One of the possible reasons for such disagreement is actually the failure of usual local approximations for exchange-correlation energy to provide accurate results for the equilibrium volume of different types of metals. In particular, the GGA, which has been used in the present theoretical investigation, works reasonably well for 3*d* metals, while it quite substantially overestimates the lattice constants of the 5*d* metals. This effect is clearly seen if one compares experimental data and theoretical results, for instance, for the first coordination shell:

Theory predicts larger separation of Pt-Pt and Fe-Pt atoms and correspondingly a smaller one for Fe-Fe pairs. Unfortunately, the use of another approximation, like the local density one, would not solve this problem since it will produce a smaller spacing between Fe atoms, although it will work better for Pt atoms. This means that it is hardly possible to resolve the existing discrepancy between theory and experiment, until a new functional, which works properly for both metals is developed.

The Invar behavior on an atomic scale has been studied in much detail on Fe-36.8 at.% Ni using diffuse x-ray scattering [8]. Interestingly, the same outcome as in this study was noted: a dependence of the static displacements (here in radial approximation) in the magnetic state is only convincingly resolvable for the first two neighboring shells. The magnitude of the species-dependent static atomic displacements at 60 K was closely reproduced by Liot and Abrikosov [7] by applying the special quasirandom structure (SQS) method [73] to model the local lattice relaxations in the lowest-energy ferromagnetic state. For an assumed nonmagnetic state, the displacements were found to differ in sign. Thus, the lower magnitudes and unchanged signs in the static displacements found experimentally at 300 K (note that at this temperature Fe-Ni is still below the Curie temperature) are very plausible.

It is striking that the long-range part of the displacement fields in Fe-Pt (Fig. 5) as well as in Fe-Ni (Ref. [8]) are quite in agreement among the respective cases beyond the nearest and next-nearest shells. This does, however, not imply that the subtle differences in subsequent shells are negligible (cf. Ref. [18]).

There is still another point to be noted on Fe-Pt: the shape of the order-disorder transition line of the Fe_3Pt phase is not symmetrical with respect to stoichiometry, as found by Osaka *et al.* [50]. This situation resembles the case of Fe-Pd on the Pd-rich side [68]. In Fe-Pd, the reason for strong shifts in congruent ordering off the 3:1 and 1:1 stoichiometry, respectively, was the composition dependence of the EPI parameters exclusively accessible from diffuse scattering. *Ab initio* electronic-structure calculations showed furthermore that the multisite interactions are strong and also possess a strong dependence on composition and configuration. Thus, a similar situation seems to be present with Fe-Pt (cf. Figs. 9 and 10).

ACKNOWLEDGMENTS

The authors are grateful to E. Fischer for his support in growing the single crystals. They also thank J. Löffler for his support and encouragement. This work was partially supported by the "Schweizerischer Nationalfonds zur Förderung der wissenschaftlichen Forschung (Project No. 200020-144461)." A.V.R.'s financial support by the Swedish Research Council (VR Project No. 15339-91505-33) and by the Austrian Federal Government (in particular from Bundesministerium für Verkehr, Innovation und Technologie and Bundesministerium für Wirtschaft, Familie und Jugend) represented by Österreichische Forschungsförderungsgesellschaft mbH and the Styrian and the Tyrolean Provincial Government, represented by Steirische Wirtschaftsförderungsgesellschaft mbH and Standortagentur Tirol, within the framework of the COMET Funding Programme, is gratefully acknowledged.

[1] Ch.-Ed. Guillaume, C. R. Hebd. Séances Acad. Sci. **125**, 235 (1897).
[2] E. F. Wassermann, in *Ferromagnetic Materials*, edited by K. H. J. Bischow and E. P. Wohlfarth (North-Holland, Amsterdam, 1990), Vol. 5, p. 237.
[3] S. Khmelevskyi and P. Mohn, Phys. Rev. B **69**, 140404(R) (2004).
[4] S. Khmelevskyi, I. Turek, and P. Mohn, Phys. Rev. Lett. **91**, 037201 (2003).
[5] S. Khmelevskyi, A. V. Ruban, Y. Kakehashi, P. Mohn, and B. Johansson, Phys. Rev. B **72**, 064510 (2005).
[6] A. V. Ruban, S. Khmelevskyi, P. Mohn, and B. Johansson, Phys. Rev. B **76**, 014420 (2007).
[7] F. Liot and I. A. Abrikosov, Phys. Rev. B **79**, 014202 (2009).
[8] J. L. Robertson, G. E. Ice, C. J. Sparks, X. Jiang, P. Zschack, F. Bley, S. Lefebvre, and M. Bessiere, Phys. Rev. Lett. **82**, 2911 (1999).
[9] G. E. Ice, C. J. Sparks, A. Habenschuss, and L. B. Shaffer, Phys. Rev. Lett. **68**, 863 (1992).
[10] X. Jiang, G. E. Ice, C. J. Sparks, L. Robertson, and P. Zschack, Phys. Rev. B **54**, 3211 (1996).
[11] Y. Tsunoda, L. Hao, S. Shimomura, F. Ye, J. L. Robertson, and J. Fernandez-Baca, Phys. Rev. B **78**, 094105 (2008).
[12] S. V. Barabash, R. V. Chepulskii, V. Blum, and A. Zunger, Phys. Rev. B **80**, 220201(R) (2009).
[13] M. Shiga, in *Material Science and Technology*, edited by R. W. Cahn, P. Haasen, and E. J. Kramer (VCH Verlagsgesellschaft, Weinheim, 1994), Vol. 3B, p. 159.
[14] K. Sumiyama, M. Shiga, M. Morioka, and Y. Nakamura, J. Phys. F: Met. Phys. **9**, 1665 (1979).
[15] K. Sumiyama, M. Shiga, and Y. Nakamura, J. Phys. Soc. Jpn. **40**, 996 (1976).
[16] M. Matsushita, S. Endo, K. Miura, and F. Ono, J. Magn. Magn. Mater. **260**, 371 (2003).
[17] M. Matsushita, S. Endo, K. Miura, and F. Ono, J. Magn. Magn. Mater. **269**, 393 (2004).
[18] Y. Tsunoda, M. Takasaka, and S. Hosoda, Phys. Rev. B **80**, 134407 (2009).
[19] A. Kußmann and G. Gräfin v. Rittberg, Zeitschrift für Metallkunde **41**, 470 (1950).
[20] E. F. Efsic and C. M. Wayman, Trans. Met. Soc. AIME **239**, 873 (1967).
[21] M. Yamamoto, S. Sekida, T. Fukuda, T. Kakeshita, K. Takahashi, K. Koyama, and H. Nojiri, J. Alloys Compds. **509**, 8530 (2011).
[22] W. Schweika, *Disordered Alloys: Diffuse Scattering and Monte Carlo Simulation*, Springer Tracts in Modern Physics No. 141 (Springer, Berlin, 1998).
[23] G. E. Ice and C. J. Sparks, Annu. Rev. Mater. Sci. **29**, 25 (1999).
[24] B. Schönfeld, Prog. Mater. Sci. **44**, 435 (1999).

[25] V. M. Nield and D. A. Keen, *Diffuse Neutron Scattering from Crystalline Materials* (Clarendon, Oxford, 2001).

[26] G. Kostorz, in *Physical Metallurgy*, edited by D. E. Laughlin and K. Hono (Elsevier, Amsterdam, 2014), p. 1227.

[27] P. Georgopoulos and J. B. Cohen, J. Phys. (Paris) Colloq. **38**, C7-191 (1977).

[28] A. V. Ruban and H. L. Skriver, Phys. Rev. B **66**, 024201 (2002); A. V. Ruban, S. I. Simak, P. A. Korzhavyi, and H. L. Skriver, *ibid.* **66**, 024202 (2002).

[29] A. V. Ruban, S. Shallcross, S. I. Simak, and H. L. Skriver, Phys. Rev. B **70**, 125115 (2004).

[30] L. Vitos, H. L. Skriver, B. Johansson, and J. Kollár, Comput. Mater. Sci. **18**, 24 (2000).

[31] L. Vitos, Phys. Rev. B **64**, 014107 (2001).

[32] L. Vitos, I. A. Abrikosov, and B. Johansson, Phys. Rev. Lett. **87**, 156401 (2001).

[33] B. L. Gyorffy, Phys. Rev. B **5**, 2382 (1972).

[34] P. Soven, Phys. Rev. **156**, 809 (1967).

[35] O. E. Peil, A. V. Ruban, and B. Johansson, Phys. Rev. B **85**, 165140 (2012); I. A. Abrikosov, A. M. N. Niklasson, S. I. Simak, B. Johansson, A. V. Ruban, and H. L. Skriver, Phys. Rev. Lett. **76**, 4203 (1996); I. A. Abrikosov, S. I. Simak, B. Johansson, A. V. Ruban, and H. L. Skriver, Phys. Rev. B **56**, 9319 (1997).

[36] J. Staunton, B. L. Gyorffy, A. J. Pindor, G. M. Stocks, and H. Winter, J. Magn. Magn. Mater. **45**, 15 (1984).

[37] B. L. Gyorffy, A. J. Pindor, J. Staunton, G. M. Stocks, and H. Winter, J. Phys. F: Met. Phys. **15**, 1337 (1985).

[38] J. P. Perdew and Y. Wang, Phys. Rev. B **45**, 13244 (1992).

[39] J. P. Perdew, K. Burke, and M. Ernzerhof, Phys. Rev. Lett. **77**, 3865 (1996).

[40] L. V. Pourovskii, A. V. Ruban, L. Vitos, H. Ebert, B. Johansson, and I. A. Abrikosov, Phys. Rev. B **71**, 094415 (2005).

[41] M. A. Krivoglaz and E. A. Tikhonova, Ukr. Fiz. Zh. (Ukr. Ed.) **3**, 297 (1958); M. A. Krivoglaz, *X-ray and Neutron Diffraction in Nonideal Crystals* (Springer, Berlin, 1996); *Diffuse Scattering of X-rays and Neutrons by Fluctuations* (Springer, Berlin, 1996).

[42] A. G. Khachaturyan, *Theory of Structural Transformations in Solids* (Wiley, New York, 1983).

[43] P. E. Blöchl, Phys. Rev. B **50**, 17953 (1994).

[44] G. Kresse and D. Joubert, Phys. Rev. B **59**, 1758 (1999).

[45] G. Kresse and J. Furthmüller, Comput. Mater. Sci. **6**, 15 (1996).

[46] G. Kresse and J. Furthmüller, Phys. Rev. B **54**, 11169 (1996).

[47] H. J. Monkhorst and J. D. Pack, Phys. Rev. B **13**, 5188 (1976).

[48] T. Sasaki and S. Chikazumi, J. Phys. Soc. Jpn. **46**, 1732 (1979).

[49] F. Arae, H. Arimune, F. Ono, and O. Yamada, J. Phys. Soc. Jpn. **54**, 3098 (1985).

[50] K. Osaka, D. Sakaki, and T. Takama, Jpn. J. Appl. Phys. **41**, L155 (2002).

[51] S. Y. Yu, B. Schönfeld, and G. Kostorz, Phys. Rev. B **56**, 8535 (1997).

[52] G. Hausch, J. Phys. Soc. Jpn. **37**, 819 (1974).

[53] *International Tables for Crystallography*, Vol. C, edited by E. Prince (International Union of Crystallography, Chester, 2006).

[54] S. Sasaki, KEK Report No. 88-14, (1989) (unpublished).

[55] B. E. Warren, *X-ray Diffraction* (Dover, New York, 1990).

[56] M. Engelke and B. Schönfeld, Acta Mater. **61**, 5087 (2013).

[57] V. Gerold and J. Kern, Acta Metall. **35**, 393 (1987).

[58] H. Okamoto, J. Phase Equilib. Diff. **25**, 395 (2004).

[59] K. Sumiyama, Y. Emoto, M. Shiga, and Y. Nakamura, J. Phys. Soc. Jpn. **50**, 3296 (1981).

[60] M. M. Abd-Elmeguid and H. Micklitz, Phys. B (Amsterdam) **163**, 412 (1990).

[61] It is interesting to note that although fully relativistic effects (due to spin-orbit coupling) correct magnetic interactions very little, they increase the Curie temperature in random Fe-25 at.% Pt by about 30 K. However, we restrict ourselves only to scalar-relativistic description in the further consideration.

[62] T. Mizoguchi, M. Akimitsu, and S. Chikazumi, J. Phys. Soc. Jpn. **34**, 932 (1973).

[63] P. A. Korzhavyi, A. V. Ruban, J. Odqvist, J.-O. Nilsson, and B. Johansson, Phys. Rev. B **79**, 054202 (2009).

[64] A. V. Ruban, P. A. Korzhavyi, and B. Johansson, Phys. Rev. B **77**, 094436 (2008).

[65] O. I. Gorbatov, I. K. Razumov, Yu. N. Gornostyrev, V. I. Razumovskiy, P. A. Korzhavyi, and A. V. Ruban, Phys. Rev. B **88**, 174113 (2013).

[66] A. V. Ruban, V. I. Baykov, B. Johansson, V. V. Dmitriev, and M. S. Blanter, Phys. Rev. B **82**, 134110 (2010).

[67] M. Rahaman, B. Johansson, and A. V. Ruban, Phys. Rev. B **89**, 064103 (2014).

[68] C. R. Sax, B. Schönfeld, and A. V. Ruban, Phys. Rev. B **89**, 014201 (2014).

[69] B. Schönfeld, G. E. Ice, C. J. Sparks, H.-G. Haubold, W. Schweika, and L. B. Shaffer, Phys. Status Solidi B **183**, 79 (1994).

[70] B. Schönfeld, L. Reinhard, G. Kostorz, and W. Bührer, Acta Mater. **45**, 5187 (1997).

[71] B. Borie and C. J. Sparks Jr., Acta Crystallogr., Sect. A: Cryst. Phys., Diffr., Theor. Gen. Crystallogr. **27**, 198 (1971).

[72] H. Maruyama, K. Shirai, H. Maeda, W.-L. Liu, and O. Yamada, J. Phys. Soc. Jpn. **56**, 4377 (1987).

[73] A. Zunger, S.-H. Wei, L. G. Ferreira, and J. E. Bernard, Phys. Rev. Lett. **65**, 353 (1990).